MONTANA STATE UNIVERSITY LIBRARY

Prokaryotes in the WAIS Divide ice core reflect source and transport changes between Last Glacial Maximum and the early Holocene

Authors: Pamela A. Santibanez, Olivia J. Maselli, Mark C. Greenwood, Mackenzie M. Grieman, Eric S. Saltzman, Joseph R. McConnell, and John C. Priscu

This is the peer reviewed version of the following article: see citation below, which has been published in Global Change Biology and found in final form at https://dx.doi.org/10.1111/gcb.14042. This article may be used for non-commercial purposes in accordance with Wiley Terms and Conditions for Self-Archiving.

Santibanez, Pamela A., Olivia J. Maselli, Mark C. Greenwood, Mackenzie M. Grieman, Eric S. Saltzman, Joseph R. McConnell, and John C. Priscu. "Prokaryotes in the WAIS Divide ice core reflect source and transport changes between Last Glacial Maximum and the early Holocene." Global Change Biology 24, no. 5 (May 2018): 2182-2197. DOI: 10.1111/gcb.14042.

Made available through Montana State University's ScholarWorks
scholarworks.montana.edu

DR. PAMELA SANTIBÁÑEZ (Orcid ID : 0000-0001-7022-3232)

Article type : Primary Research Articles

Prokaryotes in the WAIS Divide ice core reflect source and transport changes between Last Glacial Maximum and the early Holocene

Pamela A. Santibáñez [1, 2], Olivia J. Maselli[3], Mark C. Greenwood[4], Mackenzie M. Grieman[5], Eric S. Saltzman[5], Joseph R. McConnell[3] and John C. Priscu[1*]

[1]Department of Land Resources and Environmental Sciences, Montana State University, Bozeman, MT 59717, USA;

[2]Departamento Científico, Instituto Antártico Chileno (INACH), Plaza Muñoz Gamero 1055, Punta Arenas, 6200965, Chile;

[3]Desert Research Institute, Nevada System of Higher Education, Reno, NV 8512, USA;

[4]Department of Mathematical Sciences, Montana State University, Bozeman, Montana 59717, USA;

[5]Department of Earth System Science, University of California, Irvine, Irvine, California, 92697-3100, USA.

Corresponding author: John C. Priscu, +1 (406) 570-6761, jpriscu@montana.edu.

Keywords: Prokaryotes, Last Glacial Maximum, Last Deglaciation, Early Holocene, Antarctic ice core, West Antarctic Ice Sheet Divide

Accepted Article

This article has been accepted for publication and undergone full peer review but has not been through the copyediting, typesetting, pagination and proofreading process, which may lead to differences between this version and the Version of Record. Please cite this article as doi: 10.1111/gcb.14042

This article is protected by copyright. All rights reserved.

Accepted Article

Abstract

We present the first long-term, highly resolved prokaryotic cell concentration record obtained from a polar ice core. This record, obtained from the West Antarctic Ice Sheet (WAIS) Divide (WD) ice core, spanned from the Last Glacial Maximum (LGM) to the early Holocene (EH) and showed distinct fluctuations in prokaryotic cell concentration coincident with major climatic states. The time series also revealed a ~1,500-year periodicity with greater amplitude during the Last Deglaciation (LDG). Higher prokaryotic cell concentration and lower variability occurred during the LGM and EH than during the LDG. A seven-fold decrease in prokaryotic cell concentration coincided with the LGM/LDG transition and the global 19 ka meltwater pulse. Statistical models revealed significant relationships between the prokaryotic cell record and tracers of both marine (sea-salt sodium [ssNa]) and burning emissions (black carbon [BC]). Collectively, these models, together with visual observations and methanosulfidic acid (MSA) measurements, indicated that the temporal variability in concentration of airborne prokaryotic cells reflected changes in marine/sea-ice regional environments of the WAIS. Our data revealed that variations in source and transport were the most likely processes producing the significant temporal variations in WD prokaryotic cell concentrations. This record provided strong evidence that airborne prokaryotic cell deposition differed during the LGM, LDG and EH, and that these changes in cell densities could be explained by different environmental conditions during each of these climatic periods. Our observations provide the first ice core time-series evidence for a prokaryotic response to long-term climatic and environmental processes.

Introduction

Prokaryotic microorganisms (*Bacteria* and *Archaea*) represent a large portion of Earth's biosphere in terms of both abundance and biomass (Madigan et al., 2006; Whitman et

This article is protected by copyright. All rights reserved.

al., 1998). These prokaryotic domains store most of the nitrogen and phosphorus as well as half of the carbon in all living organisms on our planet (Whitman et al., 1998) and are crucial drivers of biogeochemical cycles (Falkowski et al., 2008; Field, 1998; Madsen, 2011). Consequently, understanding the ecological forces that shape microbial communities through time at different scales is essential for comprehending the response of biogeochemical cycles to climatic and environmental changes.

Polar ice cores provide archives of soluble and insoluble aerosols, gases, and their associated isotopes through time allowing examination of the historical ecological forces for timescales at which climatic and environmental processes occur. An ice core retrieved from East Antarctica (EPICA Dome Concordia ice core) yielded temporal records that have allowed reconstruction of past climatic and environmental conditions for the last ~800,000 yr (e.g., Lambert et al. 2008, Lüthi et al., 2008; Wolff et al., 2010). As biogenic aerosols, prokaryotic cells are transported and deposited onto ice sheets (Burrows et al., 2009 a, b; Jaenicke, 2005; Morris et al., 2011) in much the same manner as abiotic aerosols and become part of the ice-sheet stratigraphic record (Priscu et al., 2007; Miteva et al. 2009; Xiang et al., 2009; Liu et al. 2016). Once immured in the ice, prokaryotic cells can be preserved for thousands of years because of the subzero temperatures and low water activities within the ice matrix (Barletta et al., 2012; Hansen-Goos et al., 2014; Hodson et al., 2008; Poinar et al., 1996; Potts, 1994; Willerslev and Cooper, 2005). Although prokaryotic cells have been detected, recovered, and isolated from discrete ice-core samples (Christner et al., 2003, 2000; Miteva et al., 2004; Sheridan et al., 2003), no long-term, high-resolution temporal records exist that allow prokaryotic cell concentration to be related to the climate record.

We used flow cytometry in concert with a continuous melting system (Santibáñez et al., 2016) to produce the first temporal record of prokaryotic (non-photosynthetic members of the domains *Bacteria* and *Archaea*) cell concentration from a deep West Antarctic ice core

This article is protected by copyright. All rights reserved.

Accepted Article

(Buizert et al., 2015) spanning from 27,000 to 9,600 yr before present (27 to 9.6 ka BP). Together with other high-resolution measurements made on the same ice core, we described the temporal trends and patterns of the prokaryotic record with respect to past climatic events and evaluated the potential atmospheric sources (e.g., plants, soils, water, and rocks [Edmonds, 1979; Jones and Harrison, 2004; Kuhlman et al., 2008]) for the prokaryotic cells comprising the record. We used a Generalized Additive Model (GAM) regression to examine the relationship between prokaryotic cell concentration and sea salt sodium (ssNa), that represented a marine/sea-ice-regional source (Legrand and Mayewski, 1997; Rankin et al., 2002; Wolff et al., 2003), and non-sea salt calcium (nssCa) representing a distant terrestrial source (i.e., from other continents) (Delmonte et al., 2002; Li et al., 2008; Fischer et al., 2007b). These data were used to define key environmental factors that may have influenced temporal variations in the prokaryotic cell record between the LGM and EH.

Materials and methods

Ice-Core Regional Settings and Timescale

The West Antarctic Ice Sheet Divide (WAIS Divide: WD; 79.467° S, 112.085° W) ice core was recovered 24 km west of the Ross-Amundsen ice-flow divide and 160 km from the site of the Byrd ice core (WAIS Divide Project Members, 2013). The maximum depth of the WD core was 3,405 m, representing a temporal record that extended to ~68 ka BP. The elevation at the site during drilling was 1,766 m above sea level (a.s.l.) with a mean annual snow accumulation rate of ~22 cm a^{-1} (ice equivalent) and an average annual air temperature of -30° C. The timescale for the core (WD2014) was based on identification of annual layers to 2,850 m (back to 31.2 ka BP) using measurements of a range of annually varying chemical species in the upper 2,000 m, as well as electrical and insoluble particle measurements from 2,000 to 2,850 m (Sigl et al., 2015). The timescale has an estimated age uncertainty of 0.3%

This article is protected by copyright. All rights reserved.

(2σ) for the depth range of 1,300 m to 2,000 m, 0.6% (2σ) for the range 2,000 m to 2,300 m, and 1.8% accumulating uncertainty for the timescale between 2,300 m and 2,850 m (Sigl et al., 2015). The depth range we used to obtain the prokaryotic cell record was from 1,764 to 2,709 m.

Sample Collection

We collected discrete liquid samples from the deep WD ice core (WDC06A) using a continuous ice-core melting system (McConnell et al., 2002). To avoid contamination from the external part of the core, the samples for prokaryotic cell enumeration were taken from the center ring (inner-most 14% of the full cross-section) of a three-ring melter plate for a 1.3 cm x 1.3 cm ice core section (total area = 1.69 cm^2). To assess reproducibility and identify potential carryover by the melter system, we melted and analyzed parallel replicate sections of the ice core that corresponded to 4% of our target ice-core section (1,764–2,709 m). The replicate sections were melted days or months later than the original sections for analysis and did not show significant differences from the adjacent samples (Santibáñez et al., 2016).

A total of 594 discrete meltwater samples (1 to 8 mL each) were obtained from depths between 1,764 m and 2,684 m and fixed with formalin (2% final concentration). Prokaryotic cell concentration was determined by flow cytometry (Santibáñez et al., 2016). The samples were maintained near 4 ^{o}C during the entire sampling process. For the LGM, the mean sampling resolution was one sample per 25.4 to 98.6 cm of ice, which equated to one sample per 7.25 to 33.0 years. For the LDG, the mean resolution was one sample per 64.9 to 90.1 cm (one sample per 6.74 to 28.74 years); and for the early Holocene (EH), the mean resolution was one sample per 28.7 to 98.7 cm (one sample per 2.91 to 9.33 years; Fig. S1). The discrete prokaryotic samples were separated by uneven time intervals (Fig. S1). Annually resolved

This article is protected by copyright. All rights reserved.

accumulation rates were calculated for the WD ice core using the depth–age relationship and applying a one-dimensional, ice-flow model (Buizert et al., 2015).

Flow Cytometry

Prokaryotic cell concentration was determined using a PhytoCyt flow cytometer (Turner Designs, equivalent to the Accuri C6 BD model) installed in a Purifier horizontal clean bench with ultraviolet (UV) light (Labconco), as described in detail by Santibáñez et al. (2016). Cell concentrations were based on DNA-stained (SYTOX-green®; 0.05 μM final concentration) cells only. Santibáñez et al. (2016) provide specific details of how flow cytometry of fluorescently-stained bacterial cells differs from a traditional laser counter used to estimate dust concentration in ice cores. We use the term "prokaryotes" to represent non-photosynthetic members of the domains Bacteria and Archaea. Although our flow cytometric procedure identified photosynthetic microorganisms at a few depths, they were typically at or below the detection limit (~180 cells per sample [Santibañez et al., 2016]) and are not included in the record presented here.

The thresholds on the flow cytometer were set on the green fluorescence channel (FL1-H) at 750. Sample (2 mL) was then pipetted using sterile filtered tips from the glass vial to a clean tube with a 30 μm mesh for pre-filtration. From that tube, 150 μL was analyzed as the negative control (unstained sample), and the remaining 1800 μL was stained with SYTOX-green. A background control was obtained from the same sample vial by pipetting 300 μL into a sterile 5 mL syringe attached to a 0.22 μm pore size sterile filter (Millex ®-GV4, 4 mm filter units, 0.1 cm^2 filtration area), filtered into a falcon tube (12 x 75 mm, sterile, DNA free), and stained with SYTOX-green to a final concentration of 0.05 μM. The samples were then incubated with the stain for 20 min in the dark at room temperature. Then samples were kept at 4° C for a period no longer than 20 h before being analyzed by the flow

This article is protected by copyright. All rights reserved.

Accepted Article

cytometry. All samples were then analyzed using a flow rate of 50 µL min^{-1} with a core size of 12 µm. The samples and controls were analyzed in the following order: 250µL of blank control (Milli-Q water), 200 µL for all samples as negative controls (unstained), and background controls of 200 µL (stained 0.2 µm filtered samples). Gating strategy has been described in detail, step by step, at Santibáñez et al., (2016).

Epifluorescence Microscopy

Prokaryotic cells were enumerated by epifluorescence microscopy in 110 samples. The WD ice core samples were prepared inside a HEPA-filtered laminar-flow hood, stained with the DNA stain SYTOX-green® at a final concentration of 2.5 µM, and prokaryotic cells were quantified as described in Santibáñez et al. (2016). Prokaryotic cell sizes were measured in 15 of the samples (five samples per climatic period) (Table S1, Fig. S2). Cellular surface area was determined for ~200 cells in each sample in at least 10 randomly selected fields using Image J software. To account for differences in cell morphology, the measured two-dimensional surface area of prokaryotic cells was converted into an Equivalent Spherical Diameter (ESD). ESD is equivalent to the diameter of sphere (d) calculated based on surface area of each cell (A) (Jackson et al., 2005) using the following formula:

$$\text{ESD} = d = \sqrt{2(A/\pi)}$$

For ESD of 0.2 µm to 3.0 µm, intervals of 0.1 µm (bin size) were used to create a histogram of relative frequency (%) for each climatic period (Fig. S2).

Field Emission Scanning Electron Microscopy (FE-SEM)

Two sets of samples were prepared for FE-SEM to visualize prokaryotic cells attached to abiotic particles and prokaryotic clumps (Fig. S3-S12). Equal volumes of 45 samples from the LGM were combined to yield a 15 mL composite for the period 23.420 to

This article is protected by copyright. All rights reserved.

Accepted Article

19.978 ka BP, and equal volumes of 58 discrete samples from the LDG were combined to yield a 30 mL composite for the period 12.343 to 11.726 ka BP. These composite samples were fixed for 20 h in 5% (v/v) glutaraldehyde. Cells were then filter-concentrated onto Isopore^{TM} filters (GTBP01300, Millipore) with sterile Swinnex® filter holders. The fixed cells were dehydrated by sequential passage through an ethanol gradient ranging from 10 to 100% ethanol (in increments of 10%; 10 minutes at each concentration), dried in a Tousimis Samdri-795 critical point dryer, coated with Iridium using an Emitech K575X coater, and imaged using a Zeiss Supra 55VP FE-SEM.

Chemical Species

The chemical species used in this study – non-sea salt Ca (nssCa), sea salt Na (ssNa) and black carbon (BC) – were measured by the continuous flow analysis system adapted from McConnell et al., (2002). Total Na and Ca concentrations were measured by high-resolution inductively coupled plasma mass spectrometry (HR-ICP-MS; Thermo Element II with electrospray ionization) on an acidified (nitric acid) continuously flowing sample stream ~4 minutes after melting. Recovery of total elemental concentrations using the continuous measurement system can be <100% for more recalcitrant elements (McConnell et al., 2007a). Both Ca and Na are readily soluble, however, with the addition of ultra-pure nitric acid during the continuous flow measurement yielding 100% recoveries of these elements. BC was measured using a Single Particle Soot Photometer (SP2; Droplet Measurement Technologies) after nebulization of the meltwater stream using a Cetac AT5000+ ultrasonic nebulizer (McConnell et al., 2007b). ssNa and nssCa were computed from Na and Ca using seawater and mean sediment abundances following standard practices. The ssNa, nssCa, and BC measurements were obtained continuously and at higher resolution (effective depth resolution of ~1 cm) than prokaryotic samples (Fig. S1). Because of this disparity in

This article is protected by copyright. All rights reserved.

Accepted Article

resolution, the original sampling resolution of ssNa, nssCa, and BC were reduced to match the prokaryotic cell record allowing valid statistical comparison. We reduced the original resolution of the ssNa, nssCa, and BC by matching their sample depths to the prokaryotic sample depths and averaging the concentrations of ssNa, nssCa, and BC for prokaryotic sample depth ranges. Following this averaging protocol, 498 final data points remained for statistical comparison between cell concentration and chemical constituent concentration, with resolutions from 2.9 to 33 years.

MSA was measured on discrete samples collected using a fraction collector during the continuous WD ice-core analysis campaign. Analytical methods were similar to those recently developed for aromatic acids (Grieman et al., 2017) and included anion exchange chromatography with electrospray ionization and tandem mass spectrometric detection in negative ion mode. The analytical system consisted of a Dionex AS-AP autosampler, ICS-2100 integrated reagent-free ion chromatograph, and a ThermoFinnigan TSQ Quantum triple quadrupole mass spectrometer.

Statistical Analysis

All statistical analyses were conducted using the R-programming language (version 2.15.0 by R Foundation for Statistical Computing, 2012) with the package mgcv (Mixed GAM Computation Vehicle), version 1.7-23 (Wood & Augustin, 2002; Wood, 2011, 2006, 2004). All data is available at the US Antarctic Program Data Center (http://www.usap-dc.org/search). Then select "WAIS Divide Ice Core" from the Science Project pull-down menu. The prokaryotic cell concentration data is under the ID: 601072.

We used Generalized Additive Models (GAMs) (Hastie and Tibshirani, 1990; Wood, 2006) to describe the temporal trend of the prokaryotic cell concentration and flux time series, and to explore relationships with chemical records from the same ice core. GAMs

This article is protected by copyright. All rights reserved.

Accepted Article

provided a framework for estimating and assessing evidence for changes in the mean trend through time and were chosen over other techniques (e.g., linear regression) for four reasons. First, GAMs do not assume linearity and allow specification of the mean value of the response (Wood, 2006; Zuur et al., 2007). Second, the response variable (prokaryotic concentration, cells mL^{-1}) is based on counts; counts are often well described by a Poisson distribution. GAMs with a Poisson distribution can model the mean concentration using a log-link-function; this approach precludes the need for data transformation (Zuur et al., 2009). Third, we used a quasi-Poisson GAM because we were analyzing concentrations in an ice core and neighboring observations might have been dependent (i.e., serial correlation is expected in time series). A quasi-Poisson GAM is similar to a Poisson GAM except that the modeled variance is modified to allow for the observed overdispersion (i.e., more variability than expected in the Poisson model) that can be generated by autocorrelated responses (i.e., serial correlation). Finally, GAMs can estimate trends with unevenly spaced observations without employing data interpolation (Bellido et al. 2001; Brodeur et al., 2008; Ferry et al., 2014; Monteith et al., 2014).

The chosen covariates for GAM regression analysis were: (i) ssNa from marine/sea-ice and regional sources; (ii) nssCa from terrestrial and distant sources (i.e., primarily the southernmost areas of South America and Australia); and (iii) BC, an indicator of terrestrial biomass burning. The GAMs used a quasi-Poisson distribution (link-function = log-link) for the response (prokaryotic cell concentration), and the covariates (nssCa, ssNa and BC) were log-transformed.

GAMs also were used to infer the dominance of dry and/or wet deposition for the prokaryotic record (Alley et al., 1995; Kreutz et al., 2000). The relationship between prokaryotic concentration and snow accumulation at the drilling site (Buizert et al., 2015)

This article is protected by copyright. All rights reserved.

was estimated after adjusting for the time trend at each time span (LGM, LDG and EH) and through the entire record.

In addition to the trend analysis by GAMs, we identified periods in the prokaryotic concentration fitted trend where the slope (i.e., rate of change in the log-mean trend) was detectably different from zero using the method of finite differences (Curtis & Simpson, 2014; Monteith et al., 2014). The first derivatives of the fitted values of the trend (f_1) for a grid of 18,000 equally spaced time points were computed for the period of the WD prokaryotic record. The grid was shifted in time by a small amount (10^{-6} years), and fitted values of the trend were again determined from the model. The differences between the two sets of fitted values, divided by the difference in time, yielded the first derivatives of the trend. Uncertainty estimates also were calculated for the derivatives to form approximate 95% confidence intervals.

Along with modeling the trends through time using GAMs, we examined periodicity in the prokaryotic concentration record using the Lomb-Scargle periodogram method that provides spectral analysis of unevenly spaced time series (Lomb, 1976; Scargle, 1982; Schulz & Stattegger, 1997). The R code developed by Glynn et al., (2006) was used to estimate the periodogram and test the null hypothesis that a given spectral peak was random (i.e., no true millennial cycle signal, just noise) at each frequency. P-values were adjusted for multiple-testing using the false-discovery rate method (Glynn et al., 2006).

Results

Temporal Changes of Ice-Core Prokaryotic Cell Concentration

Prokaryotic Cell Concentration and Flux

The temporal trend in prokaryotic cell concentration was estimated by fitting a quasi-Poisson Generalized Additive Model (GAM) to the data. The trend analysis showed that the

This article is protected by copyright. All rights reserved.

Accepted Article

prokaryotic cell concentration changed significantly during the target time (p-value = 0.001, Fig. 1a) according to equation 1:

$$\log(\hat{\mu}_{prok}) = 11.61 + \mathrm{s}(time)_{78.87} \qquad \text{[eq.1]}$$

where $\hat{\mu}_{prok}$ is the mean prokaryotic cell count (cell mL^{-1}), 11.61 is the intercept (cell mL^{-1}), and s(time) denotes the smoothed trend through time. The effective degree of freedom (edf) is 78.87 and corresponds to the suitability of the estimated trend. This relatively high value of *edf* indicated a complex trend (i.e., *edf* = 0 denotes no trend, *edf* = 1 denotes a linear trend, *edf* >1 denotes a higher-order trend) (Wood, 2006; Zuur et al., 2007, 2009).

The depositional flux of prokaryotes (cells cm^{-2} a^{-1}; Fig. 1b) was calculated to evaluate the potential influence of wet deposition (i.e., snow) on prokaryotic cell concentration. The calculation used the product of the prokaryotic concentration (cells mL^{-1}; Fig. 1a) and the annual water-equivalent net accumulation (cm a^{-1}; Fig. 1c, [Buizert et al., 2015]) in the ice core. The temporal trend in depositional flux was similar to that of the prokaryotic concentration record (GAM trend as solid curve in Fig. 1b) as described by equation 2:

$$\log(\hat{\mu}_{FLUX}) = 14.39 + \mathrm{s}(time)_{72.11} \qquad \text{[eq.2]}$$

where $\hat{\mu}_{FLUX}$ = cells cm^{-2} a^{-1}; 14.39 = the y-intercept (cells cm^{-2} a^{-1}), *s(time)* = the smoothed trend through time, and 72.11 = *edf*.

This trend was statistically significant (p-value <0.01) and the *edf* of 72.11 showed that it was relatively complex. The similarity in temporal trends of cell concentration and prokaryotic cell flux (Fig. 1 a, b) indicated that the temporal changes in prokaryotic concentration were not explained by changes in snow deposition efficiency through time (e.g., lower snow accumulation during the LGM than EH). Statistical analysis showed no significant relationship between prokaryotic cell concentration and accumulation rate (Fig. 1; GAM p-value > 0.1); a similar result occurred when generalized linear models (glm) were

This article is protected by copyright. All rights reserved.

Accepted Article

applied (p-value > 0.1). This lack of a statistically significant relationship confirmed that variations in atmospheric depositional processes (wet or dry removal) were not closely associated with variations in the prokaryotic cell record. Hence, the ice concentrations of prokaryotic cells rather than depositional fluxes best represented changes in prokaryotic cell concentration in the air above the WD ice, in agreement with previous studies in the WAIS region (Alley et al., 1995; Kreutz et al., 2000).

Patterns in Prokaryotic Cell Concentration

The major patterns in the prokaryotic cell concentration coincided with the Last Glacial Maximum (LGM; 26.83 ka BP to 19.43 ka BP), the Last Deglaciation period (LDG; 19.40 ka BP to 11.60 ka BP), and the early Holocene (EH; 11.59 ka BP to 9.64 ka BP). Prokaryotic cell concentration during the LGM was higher and had lower variability (mean: 1.81 x 10^5 cells mL^{-1}; CV: 39.7%) than during the LDG (by a factor of 2.1) and the EH (by a factor of 1.4). The coldest interval in the LGM between 23.69 ka BP and 19.43 ka BP had the highest mean concentration and lowest variability (mean 2.29 x 10^5 cells mL^{-1}; CV: 30.9%). Cell concentration at the end of the LGM (~19 ka) decreased by a factor of 6.8 during 876 years with two significant steps between 19.43 and 19.05 ka BP, and 18.84 and 18.56 ka BP (derivatives of 0 not in 95% confident intervals; Fig. 1a).

Although the most distinct feature of the prokaryotic cell record was the presence of significant millennial-scale variations during the LDG, four other features characterized the prokaryotic cell record during this period: (i) the lowest mean prokaryotic concentration (8.74 x 10^4 cells mL^{-1}); (ii) the highest variability (SD = 6.7 x 10^4 cells mL^{-1}; CV = 76.8%; range = 10^3 - 10^5 cells mL^{-1}); (iii) millennial-scale cycles, and (iv) according to the analysis of the first derivatives, there were more time intervals characterized by higher rates of change in prokaryotic concentration relative to other intervals in the record (derivatives of 0 not in 95%

This article is protected by copyright. All rights reserved.

confidence intervals; Fig. 1d). The millennial-scale cycles in the LDG decreased in amplitude during the EH (~11.71 ka BP).

The mean cell concentration during the EH was 1.33 x 10^5 cells mL^{-1}, reaching the concentration values of the LGM. EH cell concentration variability decreased noticeably (SD: 5.59 x 10^4 cells mL^{-1}; CV: 41.9%) compared to the LDG period. The mean prokaryotic concentration was higher for the EH than LDG by a factor of 1.52.

Spectral Analysis

We used spectral analysis to statistically evaluate the presence of a millennial-scale cycle in the prokaryotic concentration time series (Fig. 2). Because visual observation of the data revealed an apparent cycle with a periodicity of ~1,000 years, we searched frequencies corresponding to periods from 370 years to 4,000 years. A maximum frequency of one cycle per 370 years was chosen based on sample resolution (range: 2.9–33 years, mean: 12.5 years) and time space between samples (range: 0–173.9 years, mean: 16.5). The test showed a top peak with significant periodicity at 1,494 years (frequency 0.000669; FDR-adjusted p-value < 0.01); another significant peak was obtained at lower frequencies with a periodicity of 2,847 years (frequency 0.00035; FDR-adjusted p-value < 0.01). This analysis revealed statistically significant millennial-scale oscillations throughout the prokaryotic cell concentration record (26.9 ka and 9.6 ka; Fig. 2).

Comparison with Terrestrial and Marine Aerosols

To gain further quantitative insight into the potential prokaryotic cell sources, ssNa, nssCa, BC, and time were statistically modeled as covariates. We added BC to the regression GAM because the prokaryotic trend visually paralleled trends in BC and MSA (Fig. 3), and because those trends co-varied on millennial timescales. MSA was not included in the model

This article is protected by copyright. All rights reserved.

Accepted Article

because the MSA data set was discrete, unevenly spaced, and its temporal resolution was lower (>33 years) than the prokaryotic record. Before modeling the relationships, scatterplots between prokaryotic cell as well as ssNa, nssCa, and BC concentrations on linear (Fig. 4 a, b, c) and logarithmic (Fig. 4 d, e, f) scales were examined to determine the potential relationships for each climatic interval. We chose the natural log-log relationship (Fig. 4 d, e, f) to describe the relationship between variables because (i) the unit changes in prokaryotic cell concentrations were about three orders of magnitude more than the unit changes in the covariates (nssCa, ssNa and BC), (ii) the constant variance assumption of the variables was improved by log-transformation (Fig. 4 d, e, f), and (iii) a natural log-log linear relationship between aerosols was expected if both aerosols shared source and/or air transport routes or that both were only the effect of a common third yet undefined process (Fischer et al., 2007a, b; Siggaard-Andersen, 2004). The fitted regression revealed evidence that both ssNa and BC were linked to variability (deviance explained to 58%) in the prokaryotic record (p-value < 0.05 and <0.001, respectively, n = 498) (Table 1, Fig. 5).

The relationship between prokaryotic cell concentration and ssNa (Fig. 5a) had an *edf* of 1.9 (Table 1), suggesting a higher order, non-linear relationship between prokaryotic cell concentration and ssNa. The non-linear relationship can be divided into two different behaviors. The first showed a positive linear behavior (i.e., prokaryotic cells increase as ssNa aerosols increase) only when ssNa concentrations were between 7 and ~33 ppb (Fig. 5a), inferring that the positive linear relationship between ssNa and prokaryotic cells only occurred in the LDG and EH when ssNa concentrations were < 33 ppb (Fig. 3d). The second showed that the behavior of the non-linear relationship changed when the ssNa concentration exceeded 33 ppb. Across an ssNa concentration of 33 ppb, mean changes in prokaryotic concentration were constant with a broad 95% confidence interval (Fig. 5a), indicating that prokaryotic cell concentrations did not increase when ssNa concentrations were high during

This article is protected by copyright. All rights reserved.

Accepted Article

LGM. The BC record also was significantly (p-value <0.001) related to the prokaryotic cell concentration record (Fig. 5b). An *edf* of 2.7 (Table 1) indicated a higher order, non-linear relationship between prokaryotic cell and BC concentrations. As with ssNa, the non-linear relationship had two different behaviors. First, a positive linear behavior between prokaryotic cells and BC concentrations was observed when BC concentrations were between 0.05 and 0.18 ppb, with such values observed only during the LDG (Fig. 3b). Second, the positive linear behavior ceased during the LGM and EH when the BC concentrations exceeded 0.18 ppb (Fig. 3b). Mean prokaryotic cell concentrations above that value were constant (Fig. 5b), indicating that although higher values of BC concentration (> 0.18 ppb) occurred, prokaryotic cell concentrations during the LGM and EH did not increase. In contrast to the ssNa and BC aerosol concentrations, the nssCa record (representing distant terrestrial sources) did not show covariance with the prokaryotic cell concentration (p-value = 0.574; Table 1; Fig. 4 b, e). The lack of statistical relationship between nssCa and prokaryotic cells implied that distant terrestrial soils were not significant sources of prokaryotic cells in the WD ice core and cannot explain the temporal variability of the WD prokaryotic record (Fig. 4 b, e).

Microscopic Analysis

Microscopic inspection of 110 WD samples revealed the presence of prokaryotic cell aggregates (~7 μm) between 12.45 and 10.95 ka BP and prokaryotic cells attached to sediments (>12 μm) between 26.81 and 18.29 ka BP (Fig. 6, S3-S12). A reliable quantitative analysis of prokaryotic aggregates was not possible because of a relatively low concentration of aggregates in samples and low sample volume available for microscopic analyses.

Cell sizes were measured in ~ 900 cells per period from five samples (Supplement Table 1), which represents 2.5% of the record. Information on cell size can provide insights about atmospheric transport pathways (e.g., long- vs. short-range) and nutrient availability at the

This article is protected by copyright. All rights reserved.

Accepted Article

source (Burrows et al., 2009b; Button et al., 1991, Chien et al., 2012; Upper & Hirano, 1991; Wolfenbarger, 1946). The means for the Equivalent Spherical Diameter (ESD) of cells during each climatic period were statistically different (one-way ANOVA, p-value < 0.01). The smallest mean prokaryotic cell ESD was measured on samples from the EH (mean: 1.18 ± 0.30 μm; Supplement Table 1), and the largest mean ESD occurred during LDG (1.36 ± 0.42 μm). The widest range of prokaryotic cell sizes occurred during the LDG (min-max [0.58 μm - 4.14 μm]) and the narrowest size range in the EH (min-max [0.55 μm -1.41 μm]) (Fig. S2).

Discussion

Post-depositional effects

Price and Sowers (2004) and Price (2000) provided indirect evidence that prokaryotes could be metabolically active within ice in liquid-water veins, a post-depositional process that may complicate interpretation of the prokaryotic record (Cuffey and Patterson, 2010). This may be true for temperate glacier ice (Campen et al. 2003), basal glacial ice from Antarctic glaciers (Montross et al., 2014), and polar surface glacial ice (Hodson et al., 2008); but conditions on and within the Antarctic ice sheets are not conducive to englacial and supraglacial post-depositional processes, *in situ* metabolic activity. First, the surface temperature at WD never exceeded -31° C, and the measured borehole temperature range of the ice we sampled was between -24° and -31° C (WAIS Divide Project Members, 2013) – a range that theoretically would support little maintenance metabolic activity and no net growth (Price & Sowers, 2004). These low temperatures also would result in very little quasi-liquid layer formation (scale of nm or Å) (Hansen-Goos et al., 2014; Petrenko & Whitworth, 1999; Warren & Hudson, 2003). Second, Barletta et al. (2012) showed that pH in ice veins of shallow polar ice is highly acidic (pH ~2), and that sulfate and nitrate can reach 141 and 611 mM, respectively. Both of these conditions are not conducive to supporting active

This article is protected by copyright. All rights reserved.

Accepted Article

metabolism in most organisms (Madigan et al., 2010; White, 2007). Finally, these properties, in concert with the fact that the cell concentration data showed distinct temporal trends that corresponded to major climatic events, indicated that cell division (*in situ* net growth) within WD ice core was low or non-existent.

Source, transport, and deposition of airborne prokaryotic cells

Sources, atmospheric transport processes, and deposition were the three major factors contributing to the prokaryotic cell concentration record in ice cores (Priscu et al., 2007; Xiang et al., 2009; Liu et al. 2016).The differential contribution of each of these factors can change with changes in global climate. The interpretation of the prokaryotic cell concentration, and other constituents in ice-core records, rely heavily on our capacity to untangle which factors are causing the variations in a specific record.

The lack of a relationship between prokaryotic cell concentration and snow accumulation and the similarity in trends of prokaryotic cell flux and cell concentration (Fig. 1) observed in our study indicated that deposition did not control temporal variations of the prokaryotic cell concentration record. If we had observed a significant correlation between prokaryotic cells and snow accumulation, the implication would be that prokaryotic cells were deposited mainly by snow (wet deposition) and that as snow accumulation increased, the prokaryotic cells in the ice would increase. The lack of correlation with snow accumulation suggested that the deposition of cells over WD was a combination of wet and dry cell removal from the air mass. Thus, source and transport changes were the most likely variables producing the temporal variations in the WD prokaryotic cell concentrations.

Regional sources of airborne prokaryotic cells

Although there is a paucity of aerobiological data over Antarctica (Chong et al., 2015; Pearce et al., 2016), studies have concluded that the majority of the airborne bacteria over

This article is protected by copyright. All rights reserved.

Accepted Article

Antarctica are emitted from regional sources (i.e., within Antarctica) rather than from locations beyond the continent (Burrows et al., 2009 a, b; Hodson et al., 2010; Pearce et al., 2009; Vincent, 2000). Studies of global microbial dispersion also have established that ~90% of the bacterial cells in the air over Antarctica were emitted from Antarctic regional sources (Burrows et al., 2009b). Our results showed several lines of evidence that indicated the cells recorded in the WD ice core were from regional sources. First, the higher prokaryotic concentration (10^3 to 10^5 cells mL^{-1}) in the WD ice core relative to those from more inland sites such as surface snow from South Pole (10^2 - 10^3 cells mL^{-1}; Carpenter et al., 2000) and ice from Vostok meteoric ice (~10 – 10^2 cells mL^{-1}; Christner et al., 2006) indicated that the WD site was closer to the emission sources of prokaryotic cells. The concentrations and community sizes of bacteria along a spatial transect in Antarctica decreased with increases in latitude, altitude, and distance from the coast (Hughes, 2003; Yan et al., 2012). Reduced cell concentrations at increasing distance from the source are expected because of dilution caused by mixing with low bacterial density air parcels during transport from the source (Upper and Hirano, 1991; Wolfenbarger, 1946). Second, the significant statistical relationship between prokaryotic cell concentration and ssNa revealed that the prokaryotic signal was likely related to variations in sea-ice/marine-regional sources, which has been identified as the main source of ssNa in coastal ice core sites (e.g., Rankin et al., 2002; Wagenbach et al., 1998; Wolff et al., 2003). Third, the lack of relationship between prokaryotic cell concentration and nssCa, that is mainly from distant terrestrial sources (e.g. Fischer et al., 2007b), indicated that these sources were not a dominant factor controlling the observed variations of the prokaryotic record. Finally, the presence of large cellular aggregates (~10 μm to ~20 μm diameter) in many of our samples (Fig. 6) suggested short atmospheric residence times of those aggregates; larger atmospheric particles have been shown to be more prevalent close to the source areas (e.g., Mahowald et al., 2014; Monahan et al., 1983; Satheesh et al., 1998; Tegen

This article is protected by copyright. All rights reserved.

Accepted Article

and Lacis, 1996). Marine regional sources for airborne prokaryotic cells are in agreement with current patterns of consistent onshore winds with dominant wind direction from the Amundsen-Bellingshausen Sea region to the WAIS Divide Site from automatic weather station and ERA-Interim reanalysis data (Koffman et al., 2014), and back trajectory modeling (Masclin et al., 2013).

Prokaryotic Cell Concentration by Climatic Periods

Higher prokaryotic cell concentration coupled with low variability in cell concentration occurred during the LGM, a colder and drier period relative to the present (Braconnot et al., 2007; Schneider Von Deimling et al., 2006; WAIS Divide, 2013). Potential regional sources of prokaryotic cells during the LGM were frost flowers (centimeter-scale crystal structures formed from sea ice), polynyas (areas of open water occurring within the polar sea ice that can cover of thousands of square kilometers), and the open ocean. Frost flowers have the potential to be important sources of prokaryotic cells (Bowman and Deming, 2010) during the LGM because seasonal sea ice on which frost flowers develop (Wolff et al., 2003) reached its maximum extent during this period (Gersonde et al., 2005). Ice-free polynyas are hotspots of phytoplankton and bacterial productivity. These hotspots can emit biological aerosols (Arrigo and van Dijken, 2003; Arrigo, 2003; Martin, 2001). During the LGM, there was widespread occurrence of seasonal or perennial polynyas along the Antarctic continental margin as documented by fossil foraminiferal assemblages in marine sediments (Smith et al., 2010; Sprenk et al., 2014; Thatje et al., 2008). MSA data indicated that there was high input of marine-derived emissions during the LGM in agreement with the high prokaryotic cell concentration observed in the WD core during this period (Fig. 3). The statistical relationship between prokaryotic cell concentration and ssNa, the visual correlation with MSA, and the maximum sea-ice extent led us to conclude that regional marine sources (frost flowers,

This article is protected by copyright. All rights reserved.

Accepted Article

polynyas, open ocean) were all potential sources of airborne prokaryotic cells to the WD site during LGM.

During the most recent glacial-to-interglacial transition (LDG), every component of the climate system underwent large-scale changes, some of them at extraordinary rates, representing the largest climatic oscillations of the past 20 ka (Blanchon & Shaw, 1995; Mayewski et al., 1996; McManus et al., 2004). These changes during the LDG were mirrored by large deviations in cell concentrations, relative to those observed in the LGM and EH. Between ~19 and 11.6 ka, the record showed lower prokaryotic cell concentration (including a sudden dip at ~19.5 ka) coupled with pronounced fluctuations of the 1,490-year periodicity (Figs. 1, 2).

The sudden 6.8-fold decrease of prokaryotic concentration at ~19.5 ka BP coincided with the global LGM/LDG transition (Carlson & Clark, 2012; Clark et al., 2009, 2004) and locally with early warming at WD, the latter of which has been attributed to insolation driving Southern Ocean warming and sea-ice retreat (WAIS members, 2013). We hypothesize that perturbation of the coastal areas closest to WD (Bellingshausen and Amundsen Seas), as sources of prokaryotic cells, produced the rapid decrease of cells at 19.5 ka. These coastal zones were perturbed by different processes: a sea-level rise of at least 10 m in less than 1 ka (Yokoyama et al., 2000; Weber et al., 2011), sea-ice retreat (WAIS members, 2013), and an early retreat of the ice-sheet margin in the Bellinghausen and Amundsen Seas (Heroy & Anderson, 2007; Nakada et al., 2000; Smith, 2011; Weber et al., 2011; Larter et al., 2014; Turner et al., 2017). In glaciomarine environments, suspended solids and freshwater can affect the hydrographic properties of the photic zone of the coastal waters (Domack, 1990; Hooge & Hooge, 2002), which, in turn, can have an important influence on the microbial communities in coastal environments (Fuhrman et al., 2006).

This article is protected by copyright. All rights reserved.

Although at this stage we can only hypothesize that the coeval prokaryotic concentration decrease with local coastal changes results from marine-regional sources.

Although our statistical analysis of the data precludes causal interpretations, paleoclimate archives from both hemisphere have shown that millennial-scale climate events are a common feature of the Last Glacial and the Termination II periods (e.g., Bond, 1997; Dansgaard et al., 1993; EPICA Members et al., 2006; Henry et al., 2016). Increasing evidence shows that these millennial scale oscillations resulted from the variation in meridional redistribution of the heat between hemispheres (Broecker, 1997; Buizert et al., 2015; Stocker & Johnsen, 2003) and were propagated by oceanic processes (Barker et al., 2009; Buizert et al., 2015; Marino et al., 2015; Wolff et al., 2010). The statistically significant periodicity of ~1,500-years in the prokaryotic cell concentration record (Fig. 1, Fig. 2) supports a linkage between the prokaryotic record and ocean dynamics.

There was a mean increase of prokaryotic cell concentrations during the EH to values close to those in the LGM (Fig. 3). This relationship between the EH and LGM contrasted with that found in marine and terrestrial aerosols such as nssCa and ssNa, which showed significantly higher concentrations during the LGM and lower concentrations during the EH, a pattern explained by both source extension and transport (e.g., Fischer et al., 2007a, b). Although the length of the record during the EH (11.6 to 9.6 ka BP) precluded deeper interpretation, the same response (an increase in concentration during the EH after a decrease in the LDG) occurred in the MSA and BC records (Fig. 3). This relationship suggested that the variability observed in these records was the result of climatic processes affecting their sources rather than transport processes because transport was very different between the LGM and the EH (Fisher et al., 2007b; Kohfeld et al., 2013; Krinner and Genthon, 2003; Sime et al., 2013).

This article is protected by copyright. All rights reserved.

Accepted Article

Accepted Article

Prokaryotic Cell Concentration and BC

BC, a product of biomass burning and thus a proxy for fire activity (e.g., Bisiaux et al., 2012; Goldberg, 1985), was significantly related to cell concentration (Figs. 3, 4, 5 and Table 1). During the LDG, when BC concentrations remained below 0.18 ppb, the two records exhibited a strong positive linear relationship. Positive relationships between prokaryotic cell density and BC during the past ~70 years also have been shown in ice cores taken from glaciers in the Tibetan Plateau (Liu et al., 2016).

Two facts indicated that the strong relationship between prokaryotes and BC was not a result of a common source for both aerosols or of shared transport routes. First, BC is a proxy of long-range transport of biomass burning from low and mid-latitudes (Bisiaux et al., 2012; McConnell et al., 2007a, b), whereas the characteristics of the prokaryotic cells in WD likely had a regional source. Second, BC aerosols are at least 10 times smaller (Schwarz et al., 2008, 2012) than prokaryotic cells (~90 nm and ~1000 nm, respectively), and Stoke's settling velocities indicate that the larger cellular aerosol particles would settle faster than the smaller BC particles during transport (Tegen and Lacis, 1996). For example, particles of size 0.1, 1, and 10 μm will have theoretical deposition velocities of 0.001, 0.05, and 1 cm s^{-1}, respectively, under the same atmospheric conditions (Seinfeld & Pandis, 1998).

Although the causality of the relationship between BC and prokaryotic cell abundances cannot be resolved from our data, literature reports have shown a relation between BC and prokaryotic concentration in seawater environments (Weinbauer et al., 2017). Other studies have shown that prokaryotic cell growth and activity increase in seawater immediately after BC aerosol deposition (Cattaneo et al., 2010; Jurado et al., 2008; Malits et al., 2015; Mari et al., 2014). BC can increase bacterial abundance because it stimulates aggregation of dissolved organic matter (DOM); creating hot spots of biogeochemical transformation, adsorbing bacterial cells to those hot spots, and decreasing viral infections on bacterial cells

This article is protected by copyright. All rights reserved.

(Cattaneo et al., 2010; Malits et al., 2015; Mari et al., 2014; Weinbauer et al., 2012). A recent review (Weinbauer et al., 2017) shows that volcanic ash and BC-rich aerosols have a significant effect on microbial plankton in the sea because they are a source of nutrients and/or organic carbon, and influence aggregation processes. During a period of increased forest fires and BC deposition on the Mediterranean coast, nutrient (phosphate and nitrate) concentrations increased by 1.4- to 4-fold, bacterial production by 60%, and growth efficiency by 2.9-fold (Weinbauer et al., 2017). This evidence indicates that the prokaryotic cell concentration record reflects changes in prokaryotic abundances in the marine source, which is modulated by BC deposition in seawater.

Our study is the first to show high-resolution trends in prokaryotic cell density from the LGM to the EH from an Antarctic ice core. The principal findings from our work are: (i) airborne prokaryotic cell density in the WD ice core was significantly different during the LGM, LDG, and EH; (ii) the WD prokaryotic record likely was produced by varying combinations of dry and wet deposition between the LGM and EH; (iii) the dominant sources of airborne prokaryotic cells to WD were regional; (iv) a periodicity of ~1,500 years occurred in the prokaryotic record, with the largest amplitudes during the LDG; (v) variability in cell density during the LDG and EH was related to changes in open ocean and sea-ice regional sources (ssNa); (vi) BC and prokaryotic cell concentrations were strongly correlated. Collectively, these relationships revealed that ice cores offer a unique medium to study the dynamics of microbial aerosols during past climate shifts on our planet.

Acknowledgements

This work was supported by U.S. National Science Foundation (NSF) grants 0440943, 0839075, 0839093, and 1142166. P. Santibáñez was funded by Chile Fulbright-BIO-CONICYT Scholarship. The authors would like to thank J. D'Andrilli, L. Layman, M. Sigl,

This article is protected by copyright. All rights reserved.

Accepted Article

Accepted Article

N. Chellman, R. Grinstead, and D. Pasteris for assistance with ice-core melting and discrete sample collection, and A. Chiuchiolo, T. Ranalli, M. Skidmore, T. Vick-Majors and C. Whitlock for comments on early versions of the manuscript. The authors appreciate the support of the WAIS Divide Science Coordination Office at the Desert Research Institute, Reno, NV, USA and University of New Hampshire, USA, for the collection and distribution of the WAIS Divide ice core and related tasks (NSF Grants 0230396, 0440817, 0944348, and 0944266). Kendrick Taylor led the field effort that collected the samples. The National Science Foundation Division of Polar Programs also funded the Ice Drilling Program Office (IDPO) and Ice Drilling Design and Operations (IDDO) group for coring activities; the National Ice Core Laboratory for curation of the core; the Antarctic Support Contractor for logistics support in Antarctica; and the 109th New York Air National Guard for airlift in Antarctica.

References

Alley R, Finkel R, Nishiizumi K, Anandakrishnan S, Shuman C, Mershon G, Zielinski G, Mayewski P (1995) Changes in continental and sea-salt atmospheric loadings in central Greenland during the most recent deglaciation: model-based estimates. *Journal of Glaciology,* **41**, 503–514.

Arrigo K, van Dijken G (2003) Phytoplankton dynamics within 37 Antarctic coastal polynya systems. *Journal of Geophysical Research,* **108**, 3271.

Arrigo K (2003) Impact of iceberg C-19 on Ross Sea primary production. *Geophysical Research Letters,* **30**, OCE 2–1–OCE 2–4.

Barker S, Diz P, Vautravers M, Pike J, Knorr G, Hall IR, Broecker WS (2009) Interhemispheric Atlantic seesaw response during the last deglaciation. *Nature,* **457,** 1097–102.

This article is protected by copyright. All rights reserved.

Accepted Article

Barletta R, Priscu J, Mader H, Jones W, Roe C (2012) Chemical analysis of ice vein microenvironments: II. Analysis of glacial samples from Greenland and Antarctica. *Journal of Glaciology,* **58**, 1109–1118.

Bellido J, Pierce G, Wang J (2001) Modelling intra-annual variation in abundance of squid Loligo forbesi in Scottish waters using generalised additive models. *Fisheries Research,* **52**, 23–39.

Bisiaux M, Edwards R, McConnell J, Curran M, Van Omens T, Smith A, Neumann T, Pasteris D, Penner J, Taylor K (2012) Changes in black carbon deposition to Antarctica from two high-resolution ice core records, 1850–2000 AD. *Atmospheric Chemistry and Physics,* **12**, 4107–4115.

Blanchon P, Shaw J (1995) Reef drowning during the last deglaciation-Evidence for catastrophic sea level rise and ice-sheet collapse. *Geology,* **23**, 4–8.

Bond G (1997) A Pervasive Millennial-Scale Cycle in North Atlantic Holocene and Glacial Climates. *Science,* **278**, 1257–1266.

Bowman JS, Deming JW (2010) Elevated bacterial abundance and exopolymers in saline frost flowers and implications for atmospheric chemistry and microbial dispersal. *Geophysical Research Letters*, **37**, L13501.

Braconnot P, Otto-Bliesner B, Harrison S, Joussaume S, Peterchmitt JY, Abe-Ouchi A, Crucifix M, Driesschaert E, Fichefet TH, Hewitt CD, Kageyama M, Kitoh A, Loutre MF, Marti O, Merkel U, Ramstein G, Valdes P, Weber L, Yu Y, Zhao Y (2007) Results of PMIP2 coupled simulations of the Mid-Holocene and Last Glacial Maximum–Part 2: feedbacks with emphasis on the location of the ITCZ and mid-and high latitudes heat budget. *Climate of the Past*, **3**, 279-296.

Broecker W (1997) Thermohaline Circulation, the Achilles Heel of Our Climate System: Will Man-Made CO_2 Upset the Current Balance? *Science,* **278**, 1582–1588.

This article is protected by copyright. All rights reserved.

Accepted Article

Brodeur R, Decker M, Ciannelli L, Purcell J, Bond N, Stabeno P, Acuña E, Hunt G (2008) Rise and fall of jellyfish in the eastern Bering Sea in relation to climate regime shifts. *Progress in Oceanography,* **77**, 103–111.

Buizert C, et al (2015) Precise interpolar phasing of abrupt climate change during the last ice age. *Nature,* **520**, 661–665.

Burrows S, Elbert W, Lawrence M, Poschl U (2009a) Bacteria in the global atmosphere – Part 1: Review and synthesis of literature data for different ecosystems. *Atmospheric Chemistry and Physics,* **9**, 9263–9280.

Burrows S, Butler T, Jöckel P, Tost H, Kerkweg A, Pöschl U, Lawrence M (2009b) Bacteria in the global atmosphere – Part 2: Modelling of emissions and transport between different ecosystems. *Atmospheric Chemistry and Physics***, 9**, 10829–10881.

Button DK (1991) Biochemical basis for whole-cell uptake kinetics, specific affinity, olitrophic capacity, and the meaning of the Michaelis constant. *Applied and Environmental Microbiology,* **57**, 2033–2038.

Campen R, Sowers T, Alley R (2003) Evidence of microbial consortia metabolizing within a low-latitude mountain glacier. *Geology,* **31**, 231–234.

Carlson A, Clark P (2012) Ice sheet sources of sea level rise and freshwater discharge during the Last Deglaciation. *Reviews of Geophysics,* **50**, 1–72.

Carpenter E, Lin S, Capone D (2000) Bacterial activity in South Pole snow. *Applied and Environmental Microbiology,* **66**, 4514–4517.

Cattaneo R, Rouviere C, Rassoulzadegan F, Weinbauer MG (2010) Association of marine viral and bacterial communities with reference black carbon particles under experimental conditions: an analysis with scanning electron, epifluorescence and confocal laser scanning microscopy. *FEMS Microbiology Ecology,* **74**, 382–396.

Chien A, Hill N, Levin P (2012) Cell size control in bacteria. *Curr Biol,* **22**, R340–349.

This article is protected by copyright. All rights reserved.

Chong C-W, Pearce DA, Convey P (2015) Emerging spatial patterns in Antarctic prokaryotes *Frontiers in Microbiology*, 30 September.

Christner BC, Mosley-Thompson E, Thompson LG, Zagorodnov V, Sandman K, Reeve JN (2000) Recovery and Identification of Viable Bacteria Immured in Glacial Ice. *Icarus,* **144**, 479–485.

Christner BC, Mosley-Thompson E, Thompson LG, Reeve JN (2003) Bacterial recovery from ancient glacial ice. *Environmental Microbiology,* **5**, 433–436.

Christner B, Royston-Bishop G, Foreman C, Arnold B, Tranter M, Welch K, Lyons WB, Tsapin A, Studinger M, Priscu J (2006) Limnological conditions in Subglacial Lake Vostok, Antarctica. *Limnology and Oceanography,* **51**, 2485–2501.

Clark P, McCabe A, Mix A, Weaver A (2004) Rapid rise of sea level 19,000 years ago and its global implications. *Science,* **304**, 1141–1144.

Clark PU, Dyke AS, Shakun JD, Carlson AE, Clark J, Wohlfarth B, Mitrovica JX, Hostetler SW, McCabe AM (2009) The Last Glacial Maximum. *Science*, **325**, 710e714.

Cuffey K, Paterson W (2010) *The Physics of Glaciers*. Fourth edition. Oxford, Butterworth-Heinemann.

Curtis C, Simpson G (2014) Trends in bulk deposition of acidity in the UK, 1988-2007, assessed using additive models. *Ecological Indicators,* **37**, 274–286.

Dansgaard W, Johnsen S, Clausen H, Dahl-Jensen D, Gundestrup N, Hammer C, Hvidberg C, Steffensen J, Sveinbjrnsdottir A, Jouzel J, Bond G (1993) Evidence for general instability of past climate from a 250-kyr ice-core record. *Nature,* **364**, 218–220.

Delmonte B, Petit JR, Maggi V (2002) Glacial to Holocene implications of the new 27000-year dust record from the EPICA Dome C (East Antarctica) ice core. *Climate Dynamics,* **18**, 647–660.

This article is protected by copyright. All rights reserved.

Accepted Article

Accepted Article

Domack E, Williams C (1990) *Fine Structure and Suspended Sediment Transport in Three Antarctic Fjords*, in Contributions to Antarctic Research I (ed CR Bentley), American Geophysical Union, Washington, DC

Edmonds RL (1979) *Aerobiology: The ecological Systems Approach*. First edition. Dowden, Hutchinson and Ross, Inc. Pennsylvania, USA.

EPICA Members et al (2006) One-to-one coupling of glacial climate variability in Greenland and Antarctica. *Nature,* **444**, 195–198.

Falkowski P, Fenchel T, Delong E (2008) The microbial engines that drive Earth's biogeochemical cycles. *Science,* **320**, 1034–1039.

Ferry A, Prvan T, Jersky B, Crosta X, Armand L (2014) Statistical modeling of southern ocean marine diatom proxy and winter sea ice data: Model comparison and developments. *Progress in Oceanography,* **131**, 100–112.

Field C (1998) Primary Production of the Biosphere: Integrating Terrestrial and Oceanic Components. *Science,* **281**, 237–240.

Fischer H, Siggaard-Andersen ML, Ruth U, Röthlisberger R, Wolff EW (2007a) Glacial / Interglacial Changes in Mineral Dust and Sea-Salt Records in Polar Ice Cores: Sources, Transport, and Deposition. *Reviews of Geophysics,* **45**, 1–26.

Fischer H, et al. (2007b) Reconstruction of millennial changes in dust emission, transport and regional sea ice coverage using the deep EPICA ice cores from the Atlantic and Indian Ocean sector of Antarctica. *Earth and Planetary Science Letters,* **260**, 340–354.

Fuhrman J, Hewson I, Schwalbach M, Steele J, Brown M, Naeem S (2006) Annually reoccurring bacterial communities are predictable from ocean conditions. *Proceedings of the National Academy of Sciences of the United States,* **103**, 13104–13109.

Gersonde R, Crosta X, Abelmann A, Armand L (2005) Sea-surface temperature and sea ice distribution of the Southern Ocean at the EPILOG Last Glacial Maximum - A circum-

This article is protected by copyright. All rights reserved.

Antarctic view based on siliceous microfossil records. *Quaternary Science Reviews,* **24**, 869–896.

Glynn E, Chen J, Mushegian A (2006) Detecting periodic patterns in unevenly spaced gene expression time series using Lomb-Scargle periodograms. *Bioinformatics,* **22**, 310–316.

Goldberg E (1985) *Black Carbon in the Environment*. First edition. Wiley-Interscience Publications, John Wiley & Sons, Inc., New York, USA.

Grieman M, Aydin M, Fritzsche D, McConnell J, Opel T, Sigl M, Saltzman E (2017) Aromatic acids in a Eurasian Arctic ice core: a 3000-year proxy record of biomass burning, *Climate of the Past Discussion,* **13**, 395–410.

Hansen-Goos H, Thomson E, Wettlaufer J (2014) On the edge of habitability and the extremes of liquidity. *Planetary and Space Science,* **98**, 169–181.

Hastie T, Tibshirani R (1990) Generalized additive models. *Stat, Sci*, **1**, 297–318.

Henry L, McManus J, Curry W, Roberts N, Piotrowski A, Keigwin L (2016) North Atlantic ocean circulation and abrupt climate change during the last glaciation. *Science,* **353**, 470–474.

Heroy D, Anderson J (2007) Radiocarbon constraints on Antarctic Peninsula Ice Sheet retreat following the Last Glacial Maximum (LGM). *Quaternary Science Reviews,* **26**, 3286–3297.

Hodson AJ, Anesio AM, Tranter M, Fountain A, Osborn M, Priscu JC, Laybourn-Parry, J, Sattler B (2008) Glacial Ecosystems. *Ecological Monographs*, **78**, 41–67.

Hodson A, Cameron K, Bøggild C, Irvine-Fynn T, Langford H, Pearce D, Banwart S (2010) The structure, biological activity and biogeochemistry of cryoconite aggregates upon an arctic valley glacier: Longyearbreen, Svalbard. *Journal of Glaciology,* **56**, 349–362.

This article is protected by copyright. All rights reserved.

Accepted Article

Accepted Article

Hooge P, Hooge E (2002) *Fjord oceanographic processes in Glacier Bay, Alaska*. United States Geological Survey, prepared for the National Park Service, Glacier Bay National Park.

Hughes K (2003) Aerial dispersal and survival of sewage-derived faecal coliforms in Antarctica. *Atmospheric Environment,* **37**, 3147–3155.

Jackson G, Waite A, Boyd P (2005) Role of algal aggregation in vertical carbon export during SOIREE and in other low biomass environments. *Geophysical Research Letters,* **32**, 1–4.

Jaenicke R (2005) Abundance of cellular material and proteins in the atmosphere. *Science,* **308**, 73.

Jones AM, Harrison RM (2004) The effects of meteorological factors on atmospheric bioaerosol concentrations - A review. *Science of the Total Environment,* **326**, 151–180.

Jurado E, Dachs J, Duarte CM, Simó R (2008) Atmospheric deposition of organic and black carbon to the global oceans. *Atmospheric Environment,* **42**, 7931–7939.

Koffman BG, Kreutz KJ, Breton DJ, Kane EJ, Winski DA, Birkel SD, Kurbatov AV, Handley MJ (2014) Centennial-scale variability of the Southern Hemisphere westerly wind belt in the eastern Pacific over the past two millennia. *Climate of the Past,* **10**, 1125-1144.

Kohfeld K, Graham R, de Boer A, Sime L, Wolff E, Le Quéré C, Bopp L (2013) Southern Hemisphere westerly wind changes during the Last Glacial Maximum: Paleo-data synthesis. *Quaternary Science Reviews,* **68**, 76–95.

Kreutz K, Mayewski P, Meeker L, Twickler M, Whitlow S (2000) The effect of spatial and temporal accumulation rate variability in west Antarctica on soluble ion deposition. *Geophysical Research Letters,* **27**, 2517.

This article is protected by copyright. All rights reserved.

Accepted Article

Krinner G, Genthon C (2003) Tropospheric transport of continental tracers towards Antarctica under varying climatic conditions. *Tellus Series B Chemical and Physical Meteorology,* **55**, 54–70.

Kuhlman KR, Venkat P, La Duc MT, Kuhlman GM, McKay CP (2008) Evidence of a microbial community associated with rock varnish at Yungay, Atacama Desert, Chile. *Journal of Geophysical Research: Biogeosciences,* **113**, 1–14.

Lambert F, Delmonte B, Petit J, Bigler M, Kaufmann P, Hutterli M, Stocker T, Ruth U, Steffensen J, Maggi V (2008) Dust-climate couplings over the past 800,000 years from the EPICA Dome C ice core. *Nature,* **452**, 616–9.

Larter RD, Anderson JB, Graham AG, Gohl K, Hillenbrand CD, Jakobsson M, Johnson JS, Kuhn G, Nitsche FO, Smith JA, Witus AE, Bentley MJ, Dowdeswell JA, Ehrmann W, Klages JP, Lindow J, ÓCofaigh C, Spiegel C (2014) Reconstruction of changes in the Amundsen Sea and Bellingshausen sea sector of the West Antarctic ice sheet since the last glacial maximum. *Quaternary Science Reviews*, **100**, 55-86.

Legrand M, Mayewski PA (1997) Glaciochemistry of polar ice cores: A review. *Reviews of Geophysics,* **35**, 219–243.

Li F, Ginoux P, Ramaswamy V (2008) Distribution, transport, and deposition of mineral dust in the Southern Ocean and Antarctica: Contribution of major sources. *Journal of Geophysical Research: Atmospheres,* **113**, 1–15

Liu Y, Priscu JC, Yao T, Vick-Majors T, Xu B, Jiao N, Santibáñez P, Huang S, Wang N, Greenwood M, Michaud AB, Kang S, Wang J, Gao Q, Yang Y (2016) Bacterial responses to environmental change on the Tibetan Plateau over the past half century. *Environmental Microbiology,* **18,** 1930–941.

Lomb N (1976) Least-Squares Frequency Analysis of Unequally Spaced Data. *Astrophysics and Space Science,* **39**, 447–462.

This article is protected by copyright. All rights reserved.

Accepted Article

Lüthi D, Le Floch M, Bereiter B, Blunier T, Barnola J-M, Siegenthaler U, Raynaud D, Jouzel J, Fischer H, Kawamura K, Stocker T (2008) High-resolution carbon dioxide concentration record 650,000-800,000 years before present. *Nature,* **453**, 379–382.

Madigan M, Martinko J, Brock T (2006) Brock Biology of Microorganisms. Pearson Prentice Hall, Upper Saddle River, NJ.

Madsen E (2011) Microorganisms and their roles in fundamental biogeochemical cycles. *Current Opinion in Biotechnology,* **22**, 456–464.

Mahowald N, Albani S, Kok JF, Engelstader S, Scanza RS, Ward DS, Flanner MG (2014) The size distribution of desert dust aerosols and its impact on the Earth system. *Aeolian Research,* **15**, 53–71.

Malits A, Cattaneo R, Sintes E, Gasol J, Herndl G, Weinbauer M (2015) Potential impacts of black carbon on the marine microbial community. *Aquatic Microbial Ecology,* **75**, 27–42.

Mari X, Lefèvre J, Torréton J, Bettarel Y, Pringault O, Rochelle-Newall E, Marchesiello P, Menkes C, Rodier M, Migon C, Motegi C, Weinbauer MG, Legendre L (2014) Effects of soot deposition on particle dynamics and microbial processes in marine surface waters. *Global Biogeochemical Cycles,* 662–678.

Martin S (2001) *Polynyas*. In JH Steele, KK Turekian, and SA Thorpe, editors. Encyclopedia of ocean sciences. Academic Press, San Diego, California, USA.

Marino G, Rohling E, Rodríguez-Sanz L, Grant KM, Heslop D, Roberts, AP, Stanford J, Yu J (2015) Bipolar seesaw control on last interglacial sea level. *Nature,* **522**, 197–201.

Masclin S, Frey MM, Rogge WF, Bales RC, (2013). Atmospheric nitric oxide and ozone at the WAIS Divide deep coring site: a discussion of local sources and transport in West Antarctica. *Atmospheric Chemistry and Physics*, **13**, 8857-8877.

This article is protected by copyright. All rights reserved.

Accepted Article

Mayewski P, Twickler M, Whitlow S, Meeker L, Yang Q, Thomas J, Kreutz K, Grootes P, Morse D, Steig E, Waddington E, Saltzman E, Whung P-Y, Taylor K (1996) Climate Change during the Last Deglaciation in Antarctica. *Science,* **272**, 1636–1638.

McConnell J, Aristarain A, Banta J, Edwards P, Simões J (2007a) 20th-Century doubling in dust archived in an Antarctic Peninsula ice core parallels climate change and desertification in South America. *Proceedings of the National Academy of Sciences of the United States,* **104**, 5743–5748.

McConnell J, Edwards R, Kok G, Flanner M, Zender C, Saltzman E, Banta J, Pasteris, D, Carter M, Kahl J (2007b) 20th-century industrial black carbon emissions altered Arctic climate forcing. *Science,* **317**, 1381–1384.

McConnell J, Lamorey G, Lambert S, Taylor K (2002) Continuous ice-core chemical analyses using inductively coupled plasma mass spectrometry. *Environmental Science and Technology,* **36**, 7–11.

McManus J, Francois R, Gherardi J-M, Keigwin LD, Brown-Leger S (2004) Collapse and rapid resumption of Atlantic meridional circulation linked to deglacial climate changes. *Nature,* **428**, 834–837.

Milne G, Mitrovica J (2008) Searching for eustasy in deglacial sea-level histories. *Quaternary Science Reviews,* **27**, 2292–2302.

Miteva V, Teacher C, Sowers T, Brenchley J (2009) Comparison of the microbial diversity at different depths of the GISP2 Greenland ice core in relationship to deposition climates. *Environmental Microbiololgy,* **11**, 640–56.

Miteva V, Sheridan P, Brenchley JE (2004) Phylogenetic and Physiological Diversity of Microorganisms Isolated from a Deep Greenland Glacier Ice Core. *Applied and Environmental Microbiology,* **70**, 202–213.

This article is protected by copyright. All rights reserved.

Accepted Article

Monahan E, Fairall C, Davidson K, Boyle P (1983) Observed inter-relations between 10m winds, ocean whitecaps and marine aerosols. *Quarterly Journal of the Royal Meteorological Society,* **109**, 379–392.

Monteith D, Evans C, Henrys P, Simpson G, Malcolm I (2014) Trends in the hydrochemistry of acid-sensitive surface waters in the UK 1988-2008. *Ecological Indicators,* **37**, 287–303.

Montross S, Skidmore M, Christner B, Samyn D, Tison J-L, Lorrain R, Doyle S, Fitzsimons S (2014) Debris-rich basal ice as a microbial habitat, Taylor Glacier, Antarctica. *Geomicrobiology Journal*, **31**, 76–81.

Morris C, Sands D, Bardin M, Jaenicke R, Vogel B, Leyronas C, Ariya P, Psenner R (2011) Microbiology and atmospheric processes: Research challenges concerning the impact of airborne micro-organisms on the atmosphere and climate. *Biogeosciences,* **8**, 17–25.

Nakada M, Kimura R, Okuno J, Moriwaki K, Miura H, Maemoku H (2000) Late Pleistocene and Holocene melting history of the Antarctic ice sheet derived from sea-level variations. *Marine Geology,* **167**, 85–103.

Pearce DA, Alekhina IA, Terauds A, Wilmotte A, Quesada A, Edwards A, et al. (2016) Aerobiology over Antarctica — a new initiative for atmospheric ecology. *Frontiers in Microbiology,* **7**,16.

Pearce DA, Bridge PD, Hughes KA, Sattler B, Psenner R, Russell N (2009) Microorganisms in the atmosphere over Antarctica. *FEMS Microbiology Ecology,* **69**, 143–57.

Petrenko VF, Whitworth RW (1999) *Physics of Ice*. First edition, Oxford University Press, New York, USA.

Poinar H, Höss M, Bada J, Pääbo S (1996) Amino Acid Racemization and the Preservation of Ancient DNA. *Science* **272**, 864–866.

Potts M (1994) Desiccation tolerance of prokaryotes. *Microbiological Reviews,* 58, 755–805.

This article is protected by copyright. All rights reserved.

Accepted Article

Price P, Sowers T (2004) Temperature dependence of metabolic rates for microbial growth, maintenance, and survival. *Proceedings of the National Academy of Sciences of the United States,* **101**, 4631–6.

Price P (2000) A habitat for psychrophiles in deep Antarctic ice. *Proceedings of the National Academy of Sciences of the United States,* **97**, 1247–1251.

Priscu J, Christner B, Foreman C, Royston-Bishop G (2007) *Biological Material in Ice Cores*, in: Encyclopedia of Quaternary Sciences.

Rankin AM, Wolff EW, Martin S (2002) Frost flowers: Implications for tropospheric chemistry and ice core interpretation. *Journal of Geophysical Research,* **107**, 4683.

Santibáñez P, McConnell JR, Priscu JC (2016) A flow cytometric method to measure prokaryotic records in ice cores: an example from the West Antarctic Ice Sheet Divide drilling site. *Journal of Glaciology,* **62**, 655–673.

Satheesh S, Moorthy K, Murthy B (1998) Spatial Gradients in Aerosol Characteristics over the Arabian Sea and Indian Ocean. *Journal of Geophysical Research,* **103**, 192.

Scargle J (1982) Studies in astronomical time series analysis. II - Statistical aspects of spectral analysis of unevenly spaced data. *The Astrophysical Journal,* **263**, 835–853.

Scheffer M, Carpenter S (2003) Catastrophic regime shifts in ecosystems: linking theory to observation. *Trends in Ecology & Evolution,* **18**, 648–656.

Schneider Von Deimling T, Ganopolski A, Held H, Rahmstorf S (2006). How cold was the last Glacial maximum? *Geophysical Research Letters,* **33**, 1–5.

Schulz M, Stattegger K (1997) Spectrum: spectral analysis of unevenly spaced paleoclimatic time series. *Computers & Geosciences,* **23**, 929–945.

Schwarz J, Doherty S, Li F, Ruggiero S, Tanner C, Perring A, Gao R, Fahey D (2012) Assessing Single Particle Soot Photometer and Integrating Sphere/Integrating Sandwich

This article is protected by copyright. All rights reserved.

Accepted Article

Spectrophotometer measurement techniques for quantifying black carbon concentration in snow. *Atmospheric Measurement Techniques,* **5**, 2581–2592.

Schwarz J, Gao R, Spackman J, Watts L, Thomson D, Fahey D, Ryerson T, Peischl J, Holloway J, Trainer M, Frost G, Baynard T, Lack D, de Gouw J, Warneke C, Del Negro L (2008) Measurement of the mixing state, mass, and optical size of individual black carbon particles in urban and biomass burning emissions. *Geophysical Research Letters,* **35**, L13810.

Seinfeld J, Pandis S (1998) *Atmospheric chemistry and physics: From air pollution to climate change.* John Wiley & Sons Inc., New York.

Sheridan PP, Miteva V, Brenchley JE (2003) Phylogenetic Analysis of Anaerobic Psychrophilic Enrichment Cultures Obtained from a Greenland Glacier Ice Core. *Applied and Environmental Microbiology,* **69**, 2153–2160.

Siggaard-Andersen ML (2004) *Analysis of soluble ions from dust and sea salt over the last glacial cycle in polar deep ice cores*. Ph.D. dissertation.

Sigl M, Fudge T, Winstrup M, Cole-Dai J, Ferris D, McConnell J, Taylor K, Welten K, Woodruff T, Adolphi F, Bisiaux M, Brook E, Buizert C, Caffee M, Dunbar N, Edwards R, Geng L, Iverson N, Koffman B, Layman L, Maselli O, McGwire K, Muscheler R, Nishiizumi K, Pasteris D, Rhodes R, Sowers T (2015) The WAIS Divide deep ice core WD2014 chronology – Part 2: Annual-layer counting (0–31 ka BP). *Climate of the Past Discussion,* **11**, 3425–3474.

Sime L, Kohfeld K, Le Quéré C, Wolff E, De Boer A, Graham R, Bopp L (2013) Southern Hemisphere westerly wind changes during the Last Glacial Maximum: model-data comparison. *Quaternary Science Reviews,* **64**, 104–120.

This article is protected by copyright. All rights reserved.

Accepted Article

Smith J, Hillenbrand C, Pudsey C, Allen C, Graham A (2010) The presence of polynyas in the Weddell Sea during the Last Glacial Period with implications for the reconstruction of sea-ice limits and ice sheet history. *Earth and Planetary Science Letters,* **296**, 287–298.

Smith KL (2011) Free-drifting icebergs in the Southern Ocean: An overview. *Deep-Sea Research Part II: Topical Studies in Oceanography,* **58**, 1277–1284.

Sprenk D, Weber M, Kuhn G, Wennrich V, Hartmann T, Seelos K (2014) Seasonal changes in glacial polynya activity inferred from Weddell Sea varves. *Climate of the Past Discussion*, **9**, 5123–5156.

Stocker T, Johnsen S (2003) A minimum thermodynamic model for the bipolar seesaw. *Paleoceanography,* **18**, 1087–1098.

Tegen I, Lacis A (1996) Modeling of particle size distribution and its influence on the radiative properties of mineral dust aerosol. *Journal of Geophysical Research,* **101**, 19237–19244.

Thatje S, Hillenbrand C-D, Mackensen A, Larter RD (2008) Life hung by thread: Endurance of Antarctic fauna in glacial periods. *Ecology,* **89**, 682–692.

Turner J, Orr A, Gudmundsson GH, Jenkins A, Bingham RG, Hillenbrand CD, Bracegirdle TJ (2017) Atmosphere-ocean-ice interactions in the Amundsen Sea Embayment, West Antarctica. *Reviews of Geophysics*, **55**, 235-276.

Upper C, Hirano S (1991) Aerial dispersal of bacteria, p 75-93, In Ginzburg 652 LR (ed), Assessing ecological risks of biotechnology. Butterworth-Heinemann, 653 Stoneham, Mass.

Vincent WF (2000) Evolutionary origins of Antarctic microbiota: invasion, selection and endemism. *Antarctic Sciences,* **12**, 374–385.

This article is protected by copyright. All rights reserved.

Accepted Article

Wagenbach D, Ducroz F, Mulvaney R, Keck L, Minikin A, Legrand M, Hall JS, Wolff EW (1998) Sea-salt aerosol in coastal Antarctic regions. *Journal of Geophysical Research,* **103**, 10961.

WAIS Divide Project Members (2013) Onset of deglacial warming in West Antarctica driven by local orbital forcing. *Nature,* **500**, 440–4.

Warren SG, Hudson SR (2003) Bacterial activity in South Pole snow is questionable. *Applied and Environmental Microbiology,* **69**, 6340–41

Weber M, Clark P, Ricken W, Mitrovica J, Hostetler S, Kuhn G (2011) Interhemisheric Ice-Sheet synchronicity during the Last Glacial Maximum. *Science*, **334**, 1265–1268.

Weinbauer MG, Cattaneo R, Malits A, Motegi C, Gasol JM, Herndl GJ, Mari X, Migon C, Rassoulzadegan F (2012) Black Carbon and Microorganisms in Aquatic Systems, Ecological Modelling. Nova Science Publishers, Inc.

Weinbauer MG, Guinot B, Migon C, Malfatti F, Mari X (2017) Skyfall-neglected roles of volcano ash and black carbon rich aerosols for microbial plankton in the ocean. *Journal of Plankton Research*, 39, **187-198.**

White D (2007) *The Physiology and Biochemistry of Prokaryotes*. 3rd edition Oxford University Press.

Whitman W, Coleman D, Wiebe W (1998) Perspective Prokaryotes : The unseen majority. *Proceedings of the National Academy of Sciences of the United States*, **95**, 6578–6583.

Willerslev E, Cooper A (2005) Ancient DNA. *Proceedings. Biological Sciences,* **272**, 3–16.

Wolfenbarger D (1946) Dispersion of small organisms, distance dispersion rates of bacteria, spores, seeds, pollen and insects: incidence rates of disease and injuries. *The American Midland Naturalist Journal,* **35**, 1–152.

This article is protected by copyright. All rights reserved.

Accepted Article

Wolff E, Chappellaz J, Blunier T, Rasmussen S, Svensson A (2010) Millennial-scale variability during the last glacial: The ice core record. *Quaternary Science Reviews,* **29**, 2828–2838.

Wolff EW, Rankin AM, Röthlisberger R (2003) An ice core indicator of Antarctic sea ice production? *Geophysical Research Letters*, **30**, 2–5.

Wood SN (2006) *Generalized Additive Models: an introduction with R*. Chapman and Hall/CRC, Boca Raton, FL, USA.

Wood SN (2004) Stable and Efficient Multiple Smoothing Parameter Estimation for Generalized Additive Models. *Journal of the American Statistical Association,* **99**, 673–686.

Wood SN (2011) Fast stable restricted maximum likelihood and marginal likelihood estimation of semiparametric generalized linear models. *Journal of the Royal Statistical Society: Series B,* **73**, 3–36.

Wood S, Augustin N (2002) GAMs with integrated model selection using penalized regression splines and applications to environmental modelling. *Ecological Modelling,* **157**, 157–177.

Xiang S, Shang T, Chen Y, Yao T (2009) Deposition and postdeposition mechanisms as possible drivers of microbial population variability in glacier ice: minireview. *FEMS Microbiology Ecology,* **70**, 165–176.

Yan P, Hou S, Chen T, Ma X, Zhang S (2012) Culturable bacteria isolated from snow cores along the 1300 km traverse from Zhongshan Station to Dome A, East Antarctica. *Extremophiles,* **16**, 345–354.

Yokoyama Y, Lambeck K, De Deckker P, Johnston P, Fifield L (2000) Timing of the Last Glacial Maximum from observed sea-level minima. *Nature,* **406**, 713–6.

This article is protected by copyright. All rights reserved.

Zuur AF, Ieno EN, Smith GM (2007) *Analyzing Ecological Data*, 1st ed. Springer Science+Bussines Media, LLC, New York, USA.

Zuur AF, Ieno E, Walker N, Saveliev A, Smith G (2009) *Mixed Effects Models and Extensions in Ecology with R*. Springer Science+Bussiness media, LLC, USA.

Tables

Table 1. Summary of GAM regressions using prokaryotic cell concentration as the response variable and concentrations of ssNa, nssCa, and BC, as well as time as covariates. *edf* represents the effective degrees of freedom and corresponds to the measured amount of flexibility in the estimated trend.

Variables	**edf**	**F**	**p-value**
ssNa	1.9	0.6	0.047
nssCa	0	0	0.574
BC	2.7	1.9	0.0005
Time	23.4	12.5	<0.0001

GAM	
Deviance explained (%)	58.2
Family	Quasipoisson
Link function	Log

Figures

Figure 1. Prokaryotic cell concentration and flux between 26.83 to 9.65 ka BP. **(a)** Prokaryotic cell concentration versus time, **(b)** prokaryotic cell flux versus time. In **(a)** and **(b)** the black solid curves are the fitted line from the optimal quasi-Poisson GAM (k = 120); the gray shaded areas correspond to 95% confidence bands, and the open and closed cicles are the measured prokaryotic cell concentration and estimated flux, respectively. Y-axes are on the logarithmic scale in **(a)** and **(b)**. **(c)** Snow accumulation rate (m a^{-1} ice equivalent) is plotted as 100-point moving average. **(d)** First derivative of fitted prokaryotic cell trend from the GAM (y-axis) versus time. Fitted trend shows estimated time intervals with significantly

This article is protected by copyright. All rights reserved.

Accepted Article

higher rates of change in prokaryotic cell concentrations. Periods of higher rates of change are indicated by the colored sections of the trend (blue = decrease; red=increase). Labels on the x-axis indicate climate intervals: LGM: Last Glacial Maximum, LDG: Last Deglaciation, and EH: early Holocene.

Figure 2. Spectral density versus period (years). Millennial scale pattern of prokaryotic cell concentration estimated using the Lomb-Scargle spectral analysis. Estimated Lomb-Scargle Periodogram of uneven prokaryotic cell concentration record (log-transformed).

Figure 3. Aerosol and isotope records from WD ice core. **(a)** Prokaryotic concentration record, where the black solid curves are the fitted line of the optimal quasi-Poisson GAM (k = 120); the gray areas correspond to 95% confidence bands, and the black dots are the observed prokaryotic cell concentration, **(b)** BC concentration record plotted as a 250-point moving average, **(c)** MSA (ppb) concentration record plotted as a 20-point moving average, **(d)** sea-salt Na (ssNa, ppb) concentration record plotted as a 250-point moving average, **(e)** non-sea-salt Ca (nssCa, ppb) concentration record plotted as a 250-point moving average, and **(f)** $\delta^{18}O$ of ice (‰) plotted as 100-yr moving averages (WAIS Divide Project Members, 2013). Labels on the x-axis indicate climatic intervals: LGM: Last Glacial Maximum, LDG: Last Deglaciation, and EH: early-Holocene. Note the logarithmic scale on the y-axis for all variables except $\delta^{18}O$ of ice (‰).

Figure 4. Scatterplots of prokaryotic cell concentration versus ssNa, nssCa, and BC concentrations. Prokaryotic cell concentration versus **(a, d)** ssNa (ppb), **(b, e)** nssCa (ppb), and **(c, f)** BC (ppb). Note the linear scale (concentration) on y- and x- axes for scatterplot **(a)** through **(c)**, and the logarithmic scale (logarithmic concentration) on the y- and x- axes for

This article is protected by copyright. All rights reserved.

Accepted Article

scatterplots **(d)** to **(f)**. Symbols indicate climatic intervals: circle = Last Glacial Maximum (LGM), star = Deglaciation (LDG), and square = early Holocene (EH).

Figure 5. Prokaryotic cell concentration as a function of **(a)** ssNa (ppb) and **(b)** BC (ppb) estimated by generalized additive regression model. Grey lines represent approximate 95% confidence intervals around the covariate main effects. Tick marks on the x-axis show the density of points (498 points). Values on the y-axis reflect the estimated mean concentration holding other variables constant at their means. Note the logarithmic scale on the y- and x-axes for all variables.

Figure 6. Microscopic images of prokaryotic-aggregates from WD samples. **(a-d)** prokaryotic-clumps from LDG/EH transition (12.3–11.7 ka BP); **(e-h)** prokaryotic cells attached to sediment particles from LGM and LGM/LDG transition (26.81–18.29 ka BP). Images **a**, **b**, **e,** and **f** were obtained using a field emission electron microscope (FE-SEM). Images **c**, **d**, **g,** and **h** were obtained by epifluorescence microscope; cells (dark green shapes) were stained with a DNA dye, SYTOX green. Scale bars equal to 2 μm.

Accepted Article

This article is protected by copyright. All rights reserved.

Accepted Article

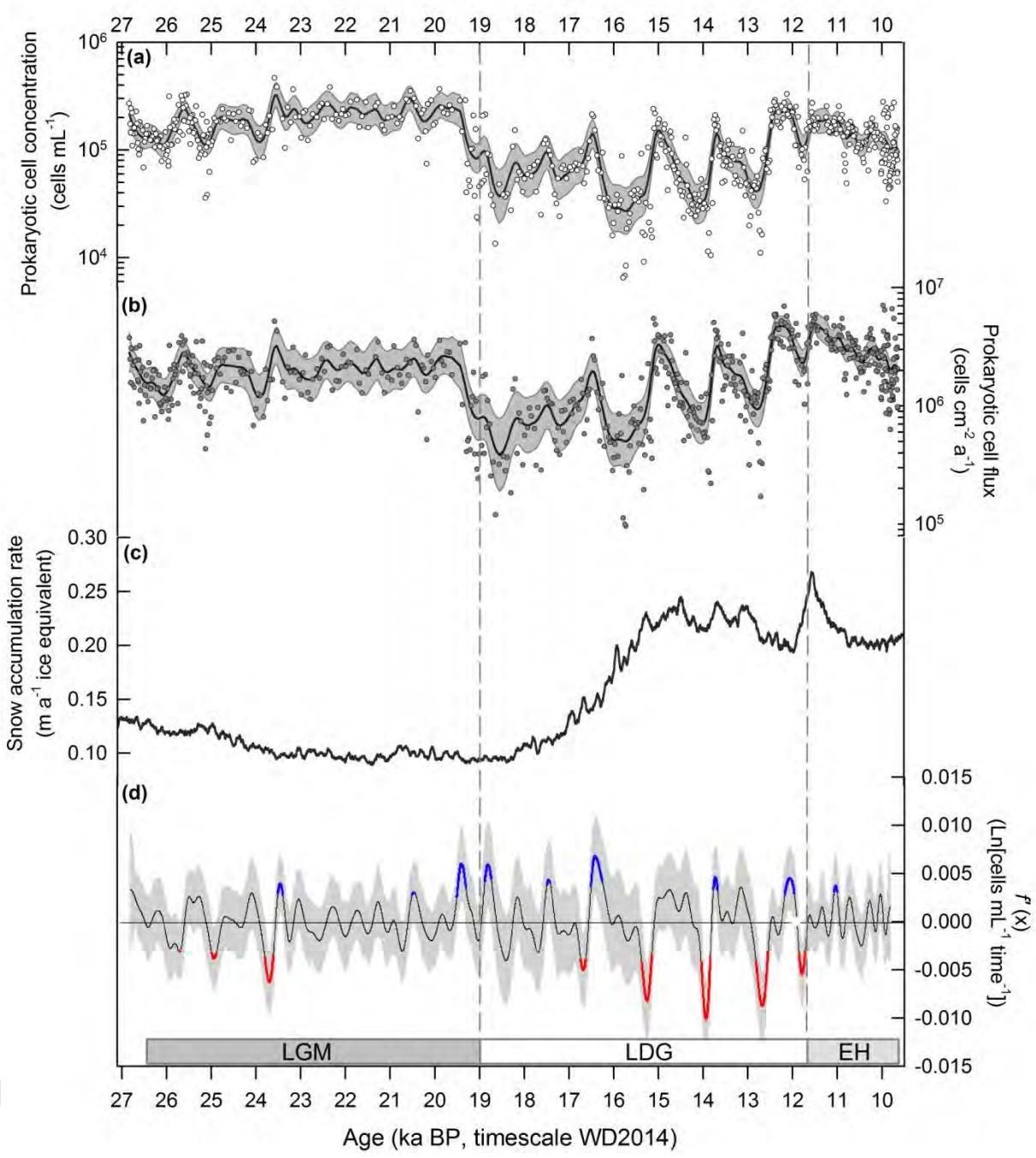

This article is protected by copyright. All rights reserved.

Accepted Article

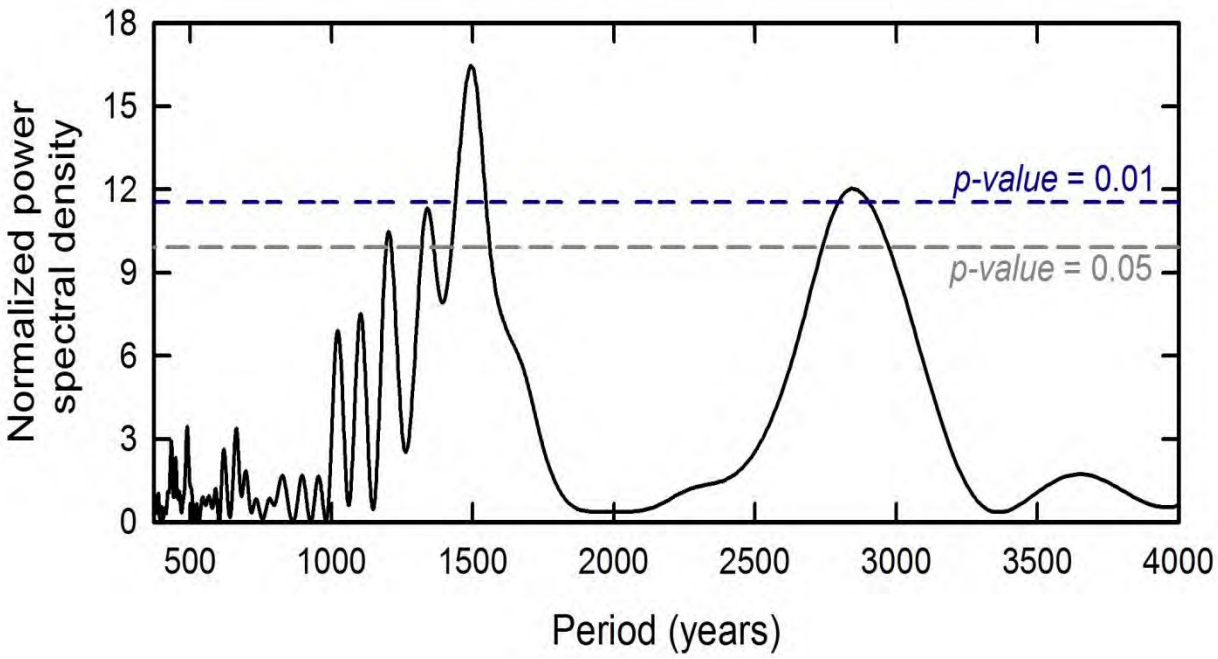

This article is protected by copyright. All rights reserved.

Accepted Article

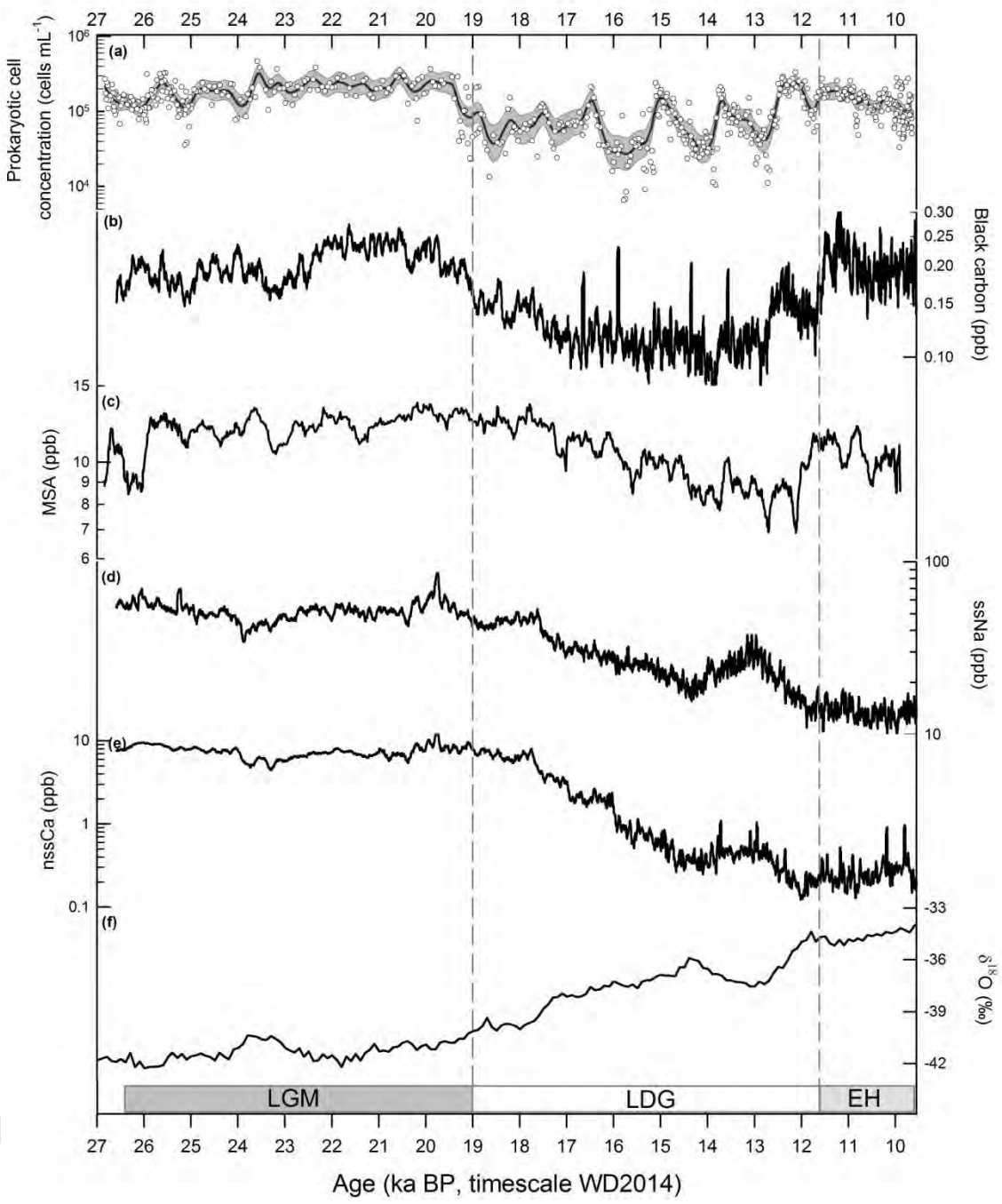

This article is protected by copyright. All rights reserved.

Accepted Article

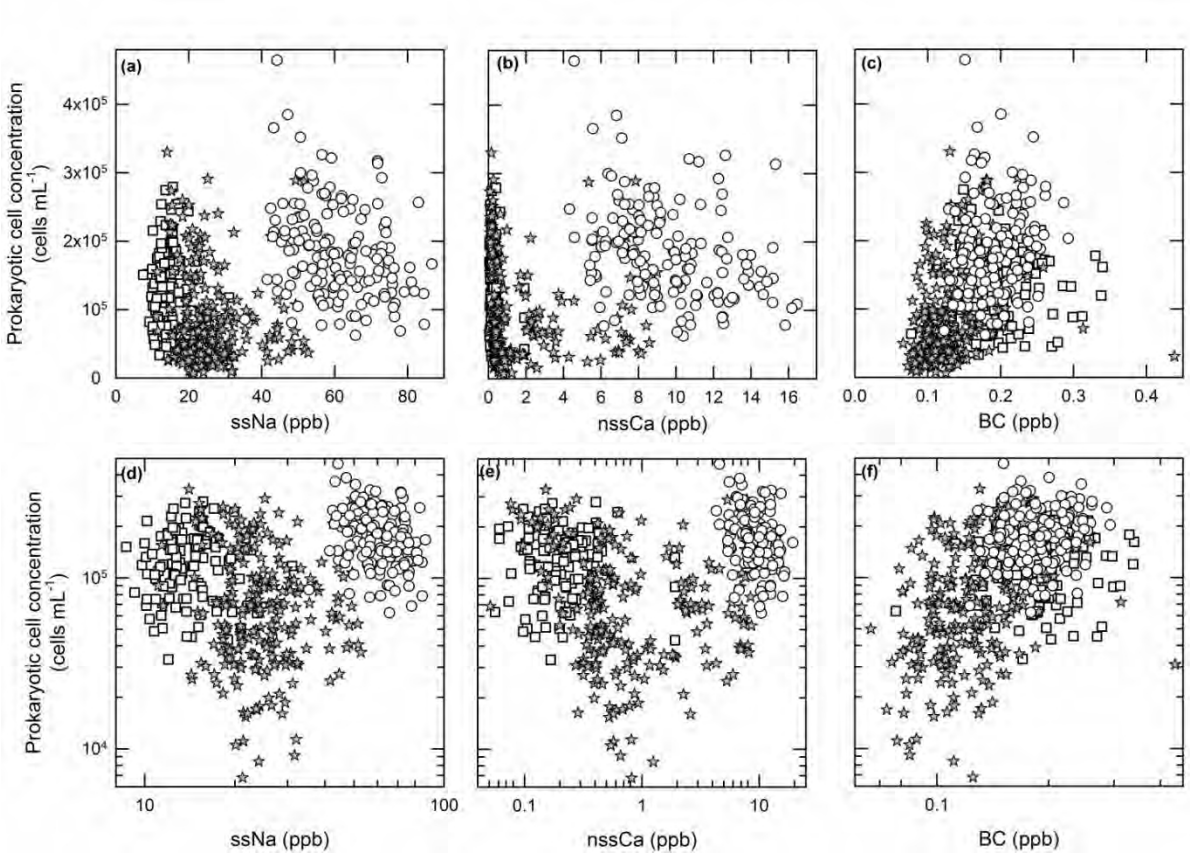

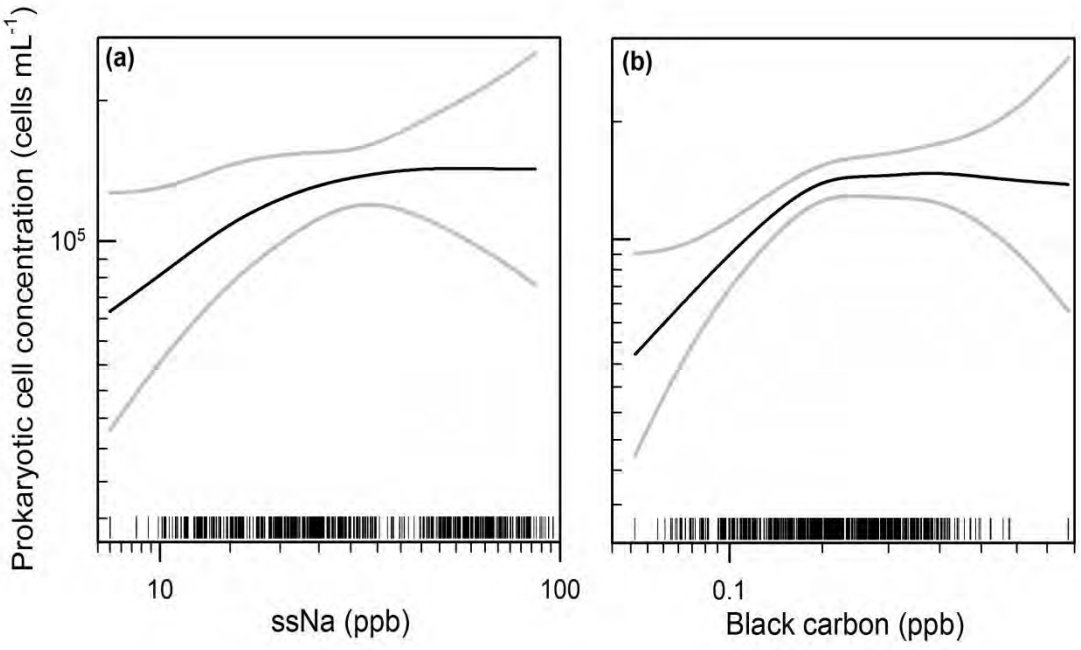

This article is protected by copyright. All rights reserved.

Accepted Article

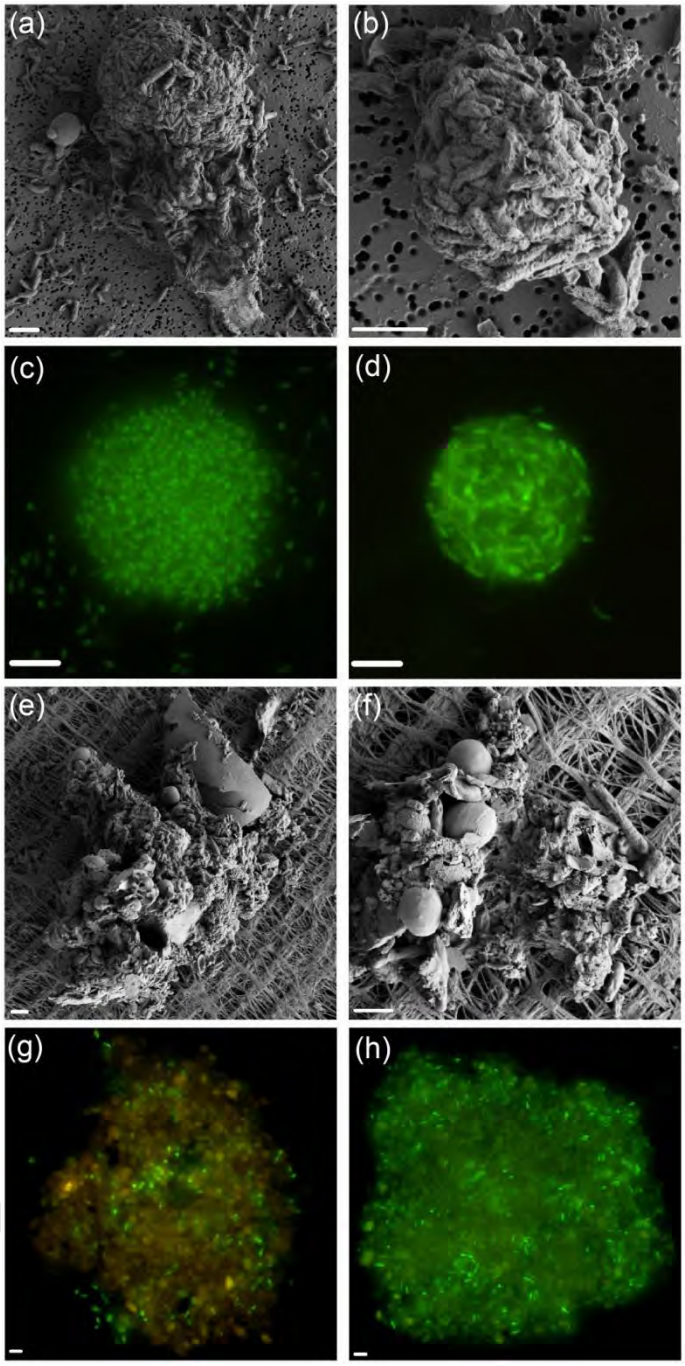

This article is protected by copyright. All rights reserved.